

# Bypassing Copyright Protection in Diffusion-based Customization via Two-Stage Latent Feature Optimization

Ziang Xu\*

220110723@stu.hit.edu.cn  
Harbin Institute of Technology,  
Shenzhen  
Shenzhen, Guangdong, China

Wenbo Yu\*

wenbo.research@gmail.com  
Tsinghua Shenzhen International  
Graduate School  
Shenzhen, Guangdong, China

Hongyao Yu

chrisqcwx@gmail.com  
Tsinghua Shenzhen International  
Graduate School  
Shenzhen, Guangdong, China

Hao Fang

fhibnese@gmail.com  
Tsinghua Shenzhen International  
Graduate School  
Shenzhen, Guangdong, China

Jiawei Kong

kjw25@mails.tsinghua.edu.cn  
Tsinghua Shenzhen International  
Graduate School  
Shenzhen, Guangdong, China

Bin Chen<sup>†</sup>

chenbin2021@hit.edu.cn  
Harbin Institute of Technology,  
Shenzhen  
Shenzhen, Guangdong, China

Hao Wu

wu-h22@mails.tsinghua.edu.cn  
Tsinghua Shenzhen International  
Graduate School  
Shenzhen, Guangdong, China

Shu-Tao Xia

xiast@sz.tsinghua.edu.cn  
Tsinghua Shenzhen International  
Graduate School  
Shenzhen, Guangdong, China

Zhiyong Wu

zywu@sz.tsinghua.edu.cn  
Tsinghua Shenzhen International  
Graduate School  
Shenzhen, Guangdong, China

## Abstract

With the growing concerns over copyright infringement in diffusion-based customization, adversarial attacks have emerged as a prominent defense strategy to prevent malicious content forgery in personalized image generation. However, current defenses typically introduce persistent perturbations in the latent space of Latent Diffusion Models (LDMs), which remain susceptible to adaptive bypasses by adversaries. In this paper, we introduce Two-Stage Latent Feature Optimization (TS-LFO), an efficient and effective copyright-stealing attack against protected diffusion-based customization. We begin by observing that existing defenses primarily disrupt the mapping between input images and their latent representations, thereby degrading the model's ability to produce personalized outputs. To counteract this, TS-LFO restores the broken mapping through a two-stage optimization process. In the Latent Denoising Stage, we enhance semantic consistency between latent codes and input images by jointly minimizing a Latent-Image Alignment Loss and a Latent Diffusion Loss with timestep-dependent weights, effectively suppressing the high-frequency noise introduced by defenses. In the Latent Reconstruction Stage, we recover low-frequency semantic information using pixel-level constraints to refine the latent features. Extensive experiments show that TS-LFO consistently bypasses state-of-the-art (SOTA) copyright defenses and outperforms SOTA copyright attacks such as DiffPure, GrIDPure and IMPRESS across diverse settings.

\*The first two authors contributed equally to this work.

<sup>†</sup> Corresponding author.



This work is licensed under a Creative Commons Attribution 4.0 International License. *KDD '26, Jeju Island, Republic of Korea*  
© 2026 Copyright held by the owner/author(s).  
ACM ISBN 979-8-4007-2259-2/2026/08  
<https://doi.org/10.1145/3770855.3817760>

## CCS Concepts

• **Security and privacy** → **Human and societal aspects of security and privacy.**

## Keywords

Copyright Concerns, Adversarial Learning, Diffusion-based Customization

## ACM Reference Format:

Ziang Xu, Wenbo Yu, Hongyao Yu, Hao Fang, Jiawei Kong, Bin Chen, Hao Wu, Shu-Tao Xia, and Zhiyong Wu. 2026. Bypassing Copyright Protection in Diffusion-based Customization via Two-Stage Latent Feature Optimization. In *Proceedings of the 32nd ACM SIGKDD Conference on Knowledge Discovery and Data Mining V.2 (KDD '26), August 09–13, 2026, Jeju Island, Republic of Korea*. ACM, New York, NY, USA, 12 pages. <https://doi.org/10.1145/3770855.3817760>

## Resource Availability:

The source code of this paper has been made publicly available at <https://doi.org/10.5281/zenodo.20508694>.

## 1 Introduction

Recent years have witnessed the rapid development and widespread application of diffusion-based generative models [3, 5, 33, 38], with representative techniques such as DreamBooth [30] and Textual Inversion [15] pushing the boundaries of personalized visual content creation. These methods enable users to synthesize high-quality images conditioned on specific visual concepts by fine-tuning diffusion models on a small number of sample images, and the continuous optimization of diffusion model architectures and training strategies has further enhanced the quality and flexibility of personalized generation. However, the powerful generative capabilities of these models also bring about prominent security and intellectual property risks: malicious users can exploit diffusion-based

customization tools to forge copyrighted visual content, counterfeit personal identities, and generate harmful information, which not only infringes on the legitimate rights and interests of content creators but also disrupts the healthy development of the generative AI ecosystem [12, 13, 25, 40]. In response to these risks, researchers have proposed adversarial perturbation-based copyright protection methods for Latent Diffusion Models (LDMs) [19, 21, 35], the core architecture of most modern diffusion-based generative systems. The core principle of these protection methods is to add targeted adversarial perturbations to images based on the loss function of diffusion model personalized training. And through such perturbations, the model’s ability to perform unauthorized personalized generation for protected content is suppressed, thus enhancing copyright protection.

Although these copyright protection methods based on diffusion model personalized training loss have demonstrated preliminary effectiveness in countering naive unauthorized generation attempts, their underlying mechanisms have not been fully explored. Through in-depth research, we have made a key finding: the adversarial perturbations added by these copyright protection methods, while suppressing unauthorized personalized generation, will objectively disrupt the stable semantic mapping relationship between protected images and their latent space representations in LDMs (i.e., the latent-image mapping). This phenomenon constitutes the foundation for existing protection methods, creating a heavy reliance on it. It also implies potential vulnerabilities of existing copyright protection strategies, which our method aims to explore and utilize. And on this basis, we design a targeted attack method to bypass the current state-of-the-art copyright protection for diffusion-based personalized generation.

In this paper, we take this important finding as the core starting point, and propose a systematic and effective attack method named Two-Stage Latent Feature Optimization (TS-LFO) to bypass the adversarial perturbation-based copyright protection methods for LDMs. The TS-LFO framework is meticulously designed to exploit the vulnerability inherent in the objective phenomenon of latent-image mapping disruption, and it achieves the unauthorized reconstruction of protected content through two stages. In the Latent Denoising Stage, we focus on eliminating the high-frequency adversarial perturbations introduced by copyright protection methods and restoring the semantic consistency between perturbed latent features and original input images. To this end, we design a novel Latent-Image Alignment Loss and a Latent Diffusion Loss with timestep-varying weight factors, which align the denoising trajectory of perturbed latent features with the natural generation process of LDMs while effectively suppressing the interference of high-frequency perturbations. In the subsequent Latent Reconstruction Stage, we leverage the structural and low-frequency semantic information that is inevitably preserved in perturbed latent features (despite the disruption of latent-image mapping) and impose pixel-level constraints to restore the low-frequency semantic fidelity of protected content, ultimately realizing the accurate reconstruction of the original protected visual content from perturbed latent representations. In summary, our main contributions are as follows:

- We propose a new copyright attack framework TS-LFO, a two-stage copyright attack that utilizes a Latent-Image Alignment Loss and a Latent Diffusion Loss with timestep-varying weight factors for high-frequency latent denoising, and utilizes pixel-level constraints for low-frequency semantic fidelity restoration.
- We analyze the robustness of copyright protections and the performance of copyright attack methods under diffusion-based customization methods. For copyright attack methods, we consider traditional adversarial defenses, advanced adversarial purification methods, and state-of-the-art (SOTA) copyright attack methods.
- Extensive experiments under various settings demonstrate that our TS-LFO can efficiently defeat SOTA copyright defenses for diffusion-based customization and outperform advanced copyright attack methods such as DiffPure, GrID-Pure and IMPRESS.

## 2 Related Works

### 2.1 Latent Diffusion Models (LDMs)

Latent Diffusion Models (LDMs) [1, 28, 32] typically comprises an autoencoder [43] and a Unet [29] denoiser. The autoencoder first encodes an input image  $x$  into a latent representation  $z = E(x)$  through its encoder  $E(\cdot)$ , while the decoder  $D(\cdot)$  learns to reconstruct the original image such that  $D(E(x)) \approx x$ . Following this, the Unet denoiser undergoes training through a noise prediction paradigm. During each timestep  $t$  in the training phase, a standard Gaussian noise sample  $\epsilon \sim \mathcal{N}(0, I)$  is first generated. The latent representation  $z$  then undergoes a forward diffusion process where the noise is progressively added to obtain  $z_t$ . Concurrently, the text prompt  $y$  is encoded into a conditional embedding  $c(y)$  using the pre-trained CLIP [27] encoder. These components (i.e., the noised latent  $z_t$ , the timestep information  $t$ , and the conditional embedding  $c(y)$ ) are jointly fed into the Unet to estimate the added noise  $\epsilon$ . The model then optimizes its parameters  $\theta$  by minimizing the expected squared error between the predicted noise and the true noise across all timesteps:

$$\mathcal{L}_{LDM} = \mathbb{E}_{z \sim E(x), y, \epsilon \sim \mathcal{N}(0, I)} [\|\epsilon - \epsilon_{\theta}(z_t, t, c(y))\|_2^2]. \quad (1)$$

During inference time, the image generation process initiates by sampling a Gaussian noise vector  $z_T \sim \mathcal{N}(0, I)$ . This noise vector then undergoes  $T$  iterative refinement steps through the trained Unet, which progressively removes the estimated noise to recover the clean latent  $z_0$ . Finally, the pre-trained decoder reconstructs the generated image by mapping the denoised latent back to the pixel space, producing the output  $x_{gen} = D(z_0)$ .

LDMs have demonstrated remarkable capabilities in generative tasks [4, 9, 26], leading to their widespread adoption across multiple domains. In the field of image synthesis, LDMs have shown superior performance in generating high-quality and diverse samples [20]. Their applications can also extend to video synthesis, where they enable temporally coherent generation through novel architectural designs [8]. For image editing tasks, LDMs provide flexible manipulation of visual content while preserving semantic consistency [18]. Notably, the success of LDMs has further expanded to 3D content creation, offering efficient text-to-3D generation pipelines

[23]. These diverse applications highlight LDMs’ versatility and effectiveness in handling various generative challenges.

## 2.2 Diffusion-based Customization

With the increasing demand for customization, numerous fine-tuning methods for diffusion models have emerged, such as DreamBooth [30] and Textual Inversion [14]. These approaches allow users to embed visual concepts into diffusion models using image modalities as input, thereby enabling the models to generate images highly similar to the input images.

**Textual Inversion** embeds concepts by training a token in the prompt, learning the embedding corresponding to that token without modifying the weights of the diffusion model.

In contrast to Textual Inversion, **DreamBooth** primarily embeds concepts by fine-tuning the weights in the Unet. First, DreamBooth introduces a prior loss to prevent overfitting. Second, it fine-tunes only the weights in the cross-attention layers of the diffusion model, as these layers are more critical for customization. Consequently, DreamBooth demonstrates superior performance and is currently the most popular customization method.

## 2.3 Copyright Protection by Adversarial Samples against Diffusion-based Customization

AdvDM [19] first proposed the idea of leveraging adversarial samples [10, 11, 37] for copyright protection against diffusion-based customization. For an input image  $x$ , the goal of AdvDM is to optimize a perturbation  $\delta$  that satisfies:

$$\|\delta\|_{\infty} < \epsilon_{LDM}, \quad \delta^* = \arg \max_{\delta} \mathcal{L}_{LDM}(x + \delta), \quad (2)$$

which will result in the adversarial sample  $x_{adv} = x + \delta^*$ . When generating images  $x_{gen}$  via diffusion-based customization methods (e.g., DreamBooth [30], Textual Inversion [15]) using  $x_{adv}$ , the generated image  $x_{gen}$  will exhibit significant discrepancies from the original image  $x$ , thereby achieving enhanced copyright protection.

Since then, many works [21, 35] have been proposed to enhance the defense robustness on the basis of AdvDM. SimAC [35] improves upon AdvDM by adding a Feature Interference Loss to the original loss function and employing a greedy timestep selection strategy, achieving better performance on facial images. DisDiff [21] incorporates a Cross-Attention Erasure module and a Merit Sampling Scheduler, which can also surpass AdvDM in terms of defense effects.

**Our Insights.** These methods fundamentally disrupt the mapping between the latent space and input images by misleading the autoencoder and the Unet [41]. Inspired by this, we propose TS-LFO, which bypasses existing copyright defenses through reconstructing the mapping between the latent space and input images, thereby enabling image copyright theft.

## 2.4 Copyright Attacks Based on Purification

While copyright protection methods such as AdvDM have achieved notable success, numerous copyright attack techniques have emerged and can circumvent these protections, thereby facilitating the theft of original image copyrights. Notable examples include DiffPure

[22], GrIDPure [45], and IMPRESS [2]. These attacks primarily leverage purification mechanisms to remove protective perturbations applied to images, restoring them to a state suitable for unauthorized use by malicious attackers.

**DiffPure** is an adversarial purification method that elegantly utilizes the noising and denoising stages of diffusion models to remove perturbations. During the noising stage, Gaussian noise is added to the adversarial example (i.e., the protected image). In the subsequent denoising stage, the pre-trained diffusion model’s prior knowledge is leveraged to jointly remove both the added Gaussian noise and the adversarial perturbations, resulting in a purified, clean image. Although DiffPure was originally designed for adversarial purification, it has proven highly effective in stripping away perturbations introduced by copyright protection mechanisms, thus functioning as a potent copyright attack.

**GrIDPure** is a copyright attack method derived from DiffPure. It enhances the purification process by dividing the adversarial input image into multiple overlapping grids. Each grid segment is individually purified using DiffPure with a relatively small diffusion timestep. The purified grid segments are then merged, typically via averaging in overlapping regions, to reconstruct the complete purified image. This grid-based approach aims to improve the efficiency and local accuracy of the purification process compared to processing the entire image at once.

**IMPRESS** is a specialized attack method designed for copyright protection techniques based on autoencoder architectures, such as PhotoGuard [31]. This method is built upon a key observation: such protection mechanisms significantly disrupt the semantic connection between the images generated by the diffusion model and the original reference image. To address this issue, IMPRESS introduces a *consistency loss*, aiming to minimize the semantic-level discrepancy between the generated image and the reference image. To circumvent the high computational cost associated with the iterative denoising process of standard diffusion models, IMPRESS employs an efficient computational framework: it bypasses the full diffusion inference chain and instead calculates the loss function using only the lightweight encoder and decoder modules from a latent diffusion model. This design substantially reduces the memory and time overhead of the optimization process. Furthermore, the method incorporates a *similarity loss* to constrain the perceptual-level structural similarity between the purified image and the original protected image, thereby ensuring the natural appearance and visual fidelity of the output.

Existing copyright attack methods (e.g., DiffPure, GrIDPure, and IMPRESS) mostly adopt a generalized purification paradigm, which attempts to *blindly* eliminate perturbations without understanding or exploiting the specific underlying mechanisms of the protection methods. Such non-targeted design strategies inherently limit the upper bound of attack effectiveness. In contrast, a profound understanding of what the protection methods actually disrupt would enable a targeted rectification of the damaged content, thereby facilitating the design of a more efficient and potent attack framework.

To address the aforementioned limitations, this paper takes the two core sub-modules of diffusion-based customization fine-tuning as a starting point to systematically investigate the internal impact mechanisms of current copyright protection methods. Guided by

these insights, we propose a highly targeted attack framework named Two-Stage Latent Feature Optimization (TS-LFO).

### 3 Method

#### 3.1 Threat Model and Evaluation of Copyright Attack

Firstly, we formally define the task of copyright infringement attacks. Suppose a copyright holder owns a clean image  $x$  but wishes to prevent it from being learned by diffusion-based customization models. To achieve this, the holder employs an advanced copyright protection method to generate a defensively perturbed image  $x_{adv}$  from  $x$  and publicly releases it. On this basis, we characterize the threat model from three distinct dimensions (i.e., attacker goal, attacker knowledge, and attacker capability) as follows:

- **Attacker Goal:** To bypass the copyright protection mechanism and leverage the publicly available perturbed images for unauthorized personalized training of diffusion models, thereby generating content that exhibits high fidelity and similarity to the original clean image  $x$ .
- **Attacker Knowledge:** The attacker has full white-box access to the underlying architecture of the latent diffusion model (including the VAE and the Unet), but possesses no prior knowledge regarding the specific copyright protection methodology employed by the holder.
- **Attacker Capability:** The attacker can only access the publicly released defensive image  $x_{adv}$  (with full operational control over it) while having no access to the original clean image  $x$ . Furthermore, the attacker retains the complete freedom to select arbitrary diffusion models to perform the infringing generation.

Under the aforementioned threat model, the objective of a malicious attacker possessing a diffusion-based customization generator  $G(\cdot)$  is to appropriately steer the generation process to obtain  $G^*(\cdot)$ .

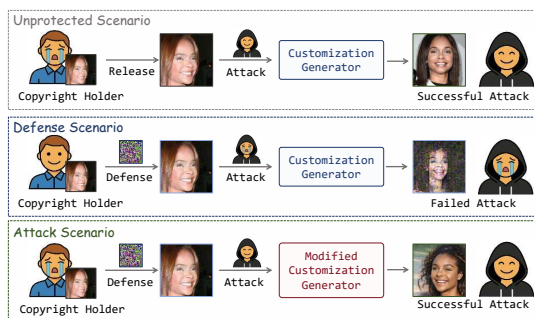


**Figure 1: An illustration of a copyright attack and defence scenario. The three rows here represent the scenario without copyright protection, the scenario with only copyright protection, and the scenario where copyright protection and copyright attack act together. We use the similarity between the clean image  $x$  held by the copyright holder and the image  $x_{gen}$  finally generated by the attacker to measure the effectiveness of the copyright attack method.**

This ensures that the new generator  $G^*(\cdot)$  can still produce an image  $x_{gen}$  highly similar to  $x$ , even when trained on the defensively perturbed image  $x_{adv}$ . The complete copyright attack and defence scenario is shown in Fig. 1, with the last column representing the copyright attack scenario that this study focuses on.

Consequently, we define the above copyright attack process as a model modification mechanism  $f: G(\cdot) \rightarrow G^*(\cdot)$ , whose effectiveness can be quantitatively measured through comparing the similarity between  $x$  and  $x_{gen}$ . Here,  $x$  is the image owned by the copyright holder in the lower left of Fig. 1, while  $x_{gen}$  is the image generated by the attacker in the lower right of Fig. 1.

To address this defined problem, we propose the Two-Stage Latent Feature Optimization (TS-LFO) method. This method modifies the process of mapping input images  $x_{adv}$  into the latent space within  $G(\cdot)$  to obtain  $x_{gen}$  with better similarity to  $x$ , thereby constituting a copyright attack. The rest of this section will elaborate on the implementation of each stage in TS-LFO.

#### 3.2 Analysis on the Mechanism of Existing Copyright Protection Methods

To design more advanced and universal copyright attack method, the key lies in deeply understanding and deconstructing the operational mechanisms of existing copyright protection methods. In real-world scenarios, attackers can only access images perturbed by defense methods, denoted as  $x_{adv}$ . Therefore, this study aims to systematically analyze how  $x_{adv}$  disrupts the functionality of core sub-modules during the personalized training of diffusion models (e.g., DreamBooth), thereby providing a theoretical foundation for designing targeted attack algorithms.

The personalized training of diffusion models primarily involves two core sub-modules: the VAE encoder  $E(\cdot)$  and the Unet denoiser  $\epsilon_\theta(\cdot)$ . The former is responsible for extracting compact latent features from input images, while the latter utilizes these features for denoising and concept learning. Based on this, we propose the following core research question: How do copyright protection perturbations separately disrupt the representational consistency of the encoder and interfere with the training dynamics of the denoiser? To address this question, we conduct empirical analyses from the following two perspectives.

##### 3.2.1 Impact of Copyright Protection on the VAE Encoder.

We find that copyright protection disrupts the mapping between the protected image and its corresponding latent features in the latent space, preventing the encoder from extracting effective latent representations from the protected image  $x_{adv}$ . In other words, the feature  $z = E(x_{adv})$  encoded from  $x_{adv}$  is a “corrupted” representation, which cannot even accurately describe the visual content of  $x_{adv}$  itself.

To quantitatively substantiate this finding, we design the following evaluation paradigm. For a given protected image  $x_{adv}$ , we reconstruct its latent feature  $z$  back into an image  $x_{rec} = D(z)$  via the VAE decoder  $D(\cdot)$ . By measuring the discrepancy  $M(x_{adv}, x_{rec})$  between the perturbed image  $x_{adv}$  and its reconstruction  $x_{rec}$ , we can directly assess the representational fidelity of the latent feature  $z$ . A larger discrepancy indicates that the perturbation causes more severe damage to the semantic consistency of the image itself and greater information loss during the encoding process. We employ a

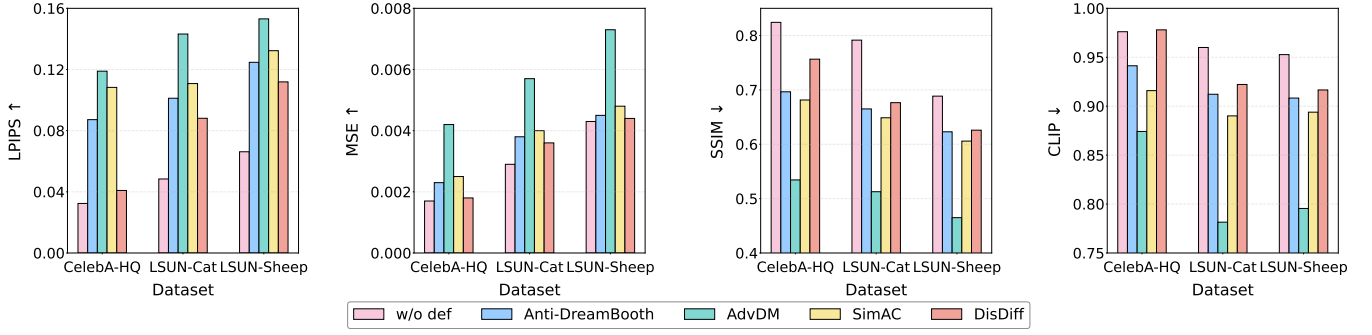


Figure 2: Comparison of the reconstructed image  $x_{rec} = D(z)$  and its corresponding input image.

complementary set of metrics  $M \in \{LPIPS, MSE, SSIM, CLIP\}$  for comprehensive evaluation, where an increase in LPIPS (perceptual difference) and MSE (mean squared error) signifies a larger discrepancy, while a decrease in SSIM (structural similarity) and CLIP (semantic similarity) scores also indicates a larger discrepancy.

We conducted experiments on three datasets (i.e., CelebA-HQ, LSUN-Cat, LSUN-Sheep) using four representative copyright protection methods (i.e., Anti-DreamBooth, AdvDM, SimAC, DisDiff) and an unprotected baseline (i.e., w/o def). The results are shown in Fig. 2. The data reveals that compared to unprotected clean images (i.e., w/o def), images  $x_{adv}$  processed by all protection methods exhibit significant representational inconsistency: their LPIPS and MSE metrics increase sharply, while their SSIM and CLIP scores drop substantially. Taking the CelebA-HQ dataset as an example, the LPIPS for w/o def is 0.0324, whereas the AdvDM method raises it to 0.1189: an increase of over 3.6 times. Its CLIP score drops from 0.9761 to 0.8742. This indicates that copyright protection severely disrupts the image-to-latent mapping in the latent space, causing the latent feature  $z$  generated by the encoder to become a “distorted” representation that fails to effectively convey the visual information of the original image.

### 3.2.2 Impact of Copyright Protection on the Unet Denoiser.

Building upon the findings about the latent representations, we further investigate the impact of the corrupted latent feature  $z$  on

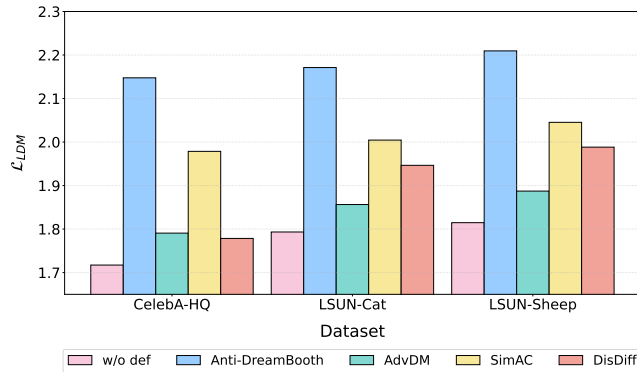


Figure 3: The impact of latent feature  $z$  on the  $\mathcal{L}_{LDM}$  under the influence of different copyright protections.

the subsequent training process of the Unet denoiser. In diffusion model training, the objective of the Unet is to predict the added noise based on a noisy latent feature. When the input training sample is the semantically inconsistent  $z$ , we hypothesize that it provides contradictory and unstable learning signals to the Unet, thereby interfering with the model’s extraction of the core features of the target concept. This ultimately manifests as optimization difficulties in the training process, namely, higher training loss.

To validate this conjecture, under the same experimental setup, we monitored the denoising loss values of the Unet during DreamBooth personalized training when using data processed by different protection methods. The results are shown in Fig. 3. The data indicates that all copyright protection methods significantly increase the Unet’s training loss. Taking the CelebA-HQ dataset as an example, the baseline loss is 1.7173, while the Anti-DreamBooth method increases it to 2.1476: a rise of approximately 25%. This result clearly supports our inference: the defects in latent representation induced by copyright protection perturbations are directly transmitted to the model training phase, significantly increasing the Unet’s training loss and hindering its efficient and accurate learning of the target visual concept.

## 3.3 The First Stage of TS-LFO: Latent Denoising Stage

### 3.3.1 Latent-Image Alignment Loss: Restore the Mapping between Protected Images and Their Latent Representations.

The analysis in Section 3.2.1 validates the necessity to obtain latent features  $z$  that closely preserve the semantic content of input. To enforce this alignment, we leverage the decoder  $D(\cdot)$  from the autoencoder with a similarity metric  $M(\cdot, \cdot)$ , formulating the loss function as:

$$\mathcal{L}_{align} = M(D(z), x_{adv}), \quad (3)$$

where  $D(\cdot)$  denotes the decoder,  $z$  is the optimized latent feature initialized as  $z = E(x_{adv})$ , and  $M(\cdot, \cdot)$  quantifies image similarity. While advanced metrics like LPIPS and SSIM are considered, counterintuitive empirical results in Section 4.4 demonstrate that traditional MSE (i.e.,  $\ell_2$  distance) outperforms them in this context.

### 3.3.2 Latent Diffusion Loss: Recover Unet Training Dynamics.

Through the quantitative analysis in Section 3.2.2, we confirm that the core negative impact of copyright protection perturbations is to significantly increase the denoising loss of the Unet during

personalized training. This finding provides a direct optimization objective for the design of copyright attack methods: an effective purified image should serve as a “high-quality training sample” for the diffusion model, thereby reducing its training loss.

To this end, we propose the Latent Diffusion Loss,  $\mathcal{L}_{DM}$ , as the core supervisory signal to guide the optimization of the attack model. This loss directly simulates and minimizes a key loss term from the downstream DreamBooth training process.

Given a latent feature  $z$  being trained, we simulate the forward noising step of the diffusion process in the latent space: randomly sample a timestep  $t \sim \mathcal{U}(1, T)$ , and add noise according to a pre-defined schedule to obtain the noisy latent feature  $z_t$ . Finally, we leverage a frozen, pre-trained Unet denoiser  $\epsilon_\theta(\cdot)$  to predict the noise added to  $z_t$  and compute the mean squared error against the actually added noise  $\epsilon$ . This is defined as the Latent Diffusion Loss:

$$\mathcal{L}_{DM} = \mathbb{E}_{t, \epsilon} [\|\epsilon_\theta(z_t, t) - \epsilon\|_2^2]. \quad (4)$$

The intuitive interpretation of this loss is: minimizing  $\mathcal{L}_{DM}$  is equivalent to optimizing the latent feature  $z$  so that, from the perspective of the pre-trained diffusion model,  $z$  itself is an easy-to-denoise, easy-to-learn feature. By directly reducing this proxy training loss, we force the optimized latent feature produced by our copyright attack method to fundamentally circumvent the interference that copyright protection imposes on the training dynamics, thereby laying the groundwork for subsequent successful personalized generation. This loss forms a closed logical loop with our previous experimental observations in Fig. 3: since copyright protection hinders learning by increasing the Unet training loss, directly optimizing against this loss constitutes the most effective attack pathway.

**3.3.3 Timestep-Varying Weight Factors: Balancing the Effects of  $\mathcal{L}_{align}$  and  $\mathcal{L}_{DM}$ .** With the two loss terms  $\mathcal{L}_{align}$  and  $\mathcal{L}_{DM}$  defined, we formulate the total loss function with a weight factor  $\lambda$ :

$$\mathcal{L} = \mathcal{L}_{align} + \lambda \mathcal{L}_{DM}. \quad (5)$$

In our preliminary experiments, we observe that for a fixed  $\lambda$ ,  $\mathcal{L}_{DM}$  naturally decays as timestep  $t$  increases, causing imbalanced optimization: the training prioritizes  $\mathcal{L}_{DM}$  reduction at smaller  $t$  but switches focus to  $\mathcal{L}_{align}$  at larger  $t$ . To enforce consistent optimization across all timesteps, we introduce timestep-dependent weight factors with linear scheduling:

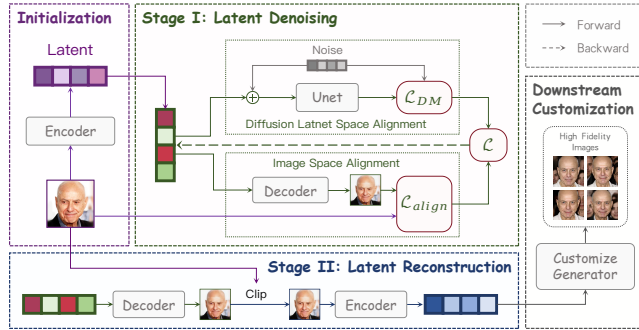


Figure 4: An overview of the complete TS-LFO pipeline, which consists of the Latent Denoising Stage, Latent Reconstruction Stage, and Downstream Customization Stage.

$$\lambda_t = \lambda_l + \frac{(\lambda_r - \lambda_l)}{T} \cdot t, \quad (6)$$

$$\mathcal{L} = \mathcal{L}_{align} + \lambda_t \mathcal{L}_{DM}. \quad (7)$$

Here  $t \sim \mathcal{U}(1, T)$  denotes the current timestep,  $T$  is the total diffusion steps, and  $\lambda_l$  and  $\lambda_r$  represent the initial and final weight factors (typically set to  $1 \times 10^{-4}$  and  $3 \times 10^{-3}$  respectively).

### 3.4 The Second Stage of TS-LFO: Latent Reconstruction Stage

Unlike classification tasks, diffusion-based customization is a generative task where output quality critically depends on the input image quality. We validate this by training Textual Inversion with three image sets: clear images, blurry images, and more blurry images. As shown in Fig. 5, the FID scores between generated images and clear images exhibit a clear increasing trend from 159.50 to 177.25 and 207.58. This indicates that the input quality significantly affects the output quality.

After conducting the first stage, we obtain an optimized latent feature  $z$  that retains semantic similarity to the input  $x_{adv}$  but with reduced quality. To enhance  $z$ 's quality while preserving similarity to  $x_{adv}$ , we exert pixel-level constraints to obtain  $z_{new}$ :

$$z_{new} = E(\text{clamp}(D(z), x_{adv} - \epsilon_{rec}, x_{adv} + \epsilon_{rec})), \quad (8)$$

where  $z_{new}$  is the reconstructed latent feature,  $\text{clamp}(\cdot, \cdot, \cdot)$  is the cropped function, and  $\epsilon_{rec}$  controls the reconstruction range. Here,  $\epsilon_{rec}$  is a hyperparameter, typically set to  $8/255$ .

This constraint ensures the semantic meaning of optimized  $z$  does not deviate significantly from  $x$ , thereby maintaining latent quality. Although minor defensive perturbations may persist in  $z$ , they have negligible impact on the LDMs' training. Experimental validation is provided in Section 4.4. An overview of the complete TS-LFO pipeline is illustrated in Fig. 4.

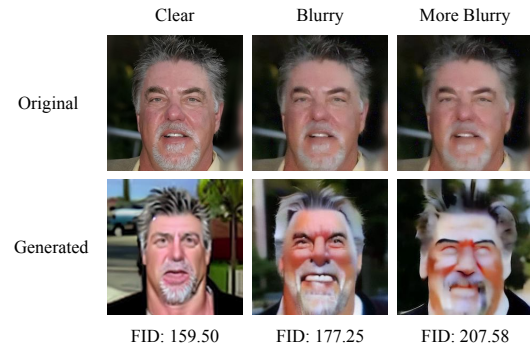


Figure 5: We train Textual Inversion with three image sets (i.e., clear images, blurry images, and more blurry images). This increasing trend in FID indicates that the quality of the input image determines the quality of the generated image.

**Table 1: (DreamBooth) The performance of our method on SOTA defenses.**

Dataset	Metric	w/o def	Anti-DreamBooth		AdvDM		SimAC		DisDiff	
			w/ def	TS-LFO	w/ def	TS-LFO	w/ def	TS-LFO	w/ def	TS-LFO
LSUN-cat	FID ↓	234.52	339.78	<b>243.62</b>	401.08	<b>249.94</b>	362.01	247.57	327.16	<b>244.12</b>
	CLIP <sub>img</sub> ↑	0.8228	0.7048	<b>0.8135</b>	0.6353	<b>0.7802</b>	0.6832	<b>0.8093</b>	0.7313	<b>0.8175</b>
	LPIPS ↓	0.4976	0.6278	<b>0.5109</b>	0.5612	<b>0.5134</b>	0.6237	<b>0.5065</b>	0.5783	<b>0.5072</b>
CelebA-HQ	FID ↓	172.42	364.30	<b>167.75</b>	237.00	<b>181.34</b>	306.78	170.15	175.03	<b>165.86</b>
	CLIP <sub>img</sub> ↑	0.8020	0.6358	<b>0.7519</b>	0.6878	<b>0.7564</b>	0.6647	<b>0.8031</b>	0.7886	<b>0.8028</b>
	LPIPS ↓	0.4901	0.7000	<b>0.5148</b>	0.5187	<b>0.4687</b>	0.6333	<b>0.4789</b>	0.5037	<b>0.4757</b>
LSUN-sheep	FID ↓	297.63	369.24	<b>303.08</b>	417.33	<b>306.16</b>	414.84	<b>301.74</b>	395.20	<b>304.83</b>
	CLIP <sub>img</sub> ↑	0.7942	0.7064	<b>0.7700</b>	0.6244	<b>0.7476</b>	0.6591	<b>0.7827</b>	0.6883	<b>0.7818</b>
	LPIPS ↓	0.4953	0.5961	<b>0.5103</b>	0.5602	<b>0.5179</b>	0.6020	<b>0.5084</b>	0.5784	<b>0.5052</b>

## 4 Experiments

### 4.1 Experimental Setup

**Datasets.** We choose three datasets: CelebA-HQ [17] (face dataset), LSUN-cat [39], and LSUN-sheep [39].

**Defense Baseline.** We select open-source copyright protection methods using adversarial samples against diffusion-based customization: Anti-DreamBooth [34], AdvDM [19], SimAC [35], DisDiff [21], and PhotoGuard [31].

**Attack Baseline.** We select SOTA adversarial purification method DiffPure [22], and the advanced copyright attack methods IMPRESS [2] and GrIDPure [45]. The method of adding Gaussian noise is also chosen as a representative of traditional copyright attacks.

**Metrics.** We evaluate similarity between generated and original images using FID [16] (lower ↓ better), CLIP [27] Image-Image Similarity (higher ↑ better), and LPIPS [42] (lower ↓ better). Higher similarity indicates more successful copyright theft. For the face dataset, we additionally introduce two metrics: FDFR (lower ↓ better) and ISM (higher ↑ better). FDFR is designed to measure whether the generated results contain valid facial structures, obtained by calculating the proportion of images in which no face can be detected after processing by the RetinaFace [6] face detection model. ISM, on the other hand, is used to assess the identity consistency between the generated face and the target user. It is computed by employing the ArcFace [7] model to extract identity feature vectors from the generated face and all original clean images of the user, followed by calculating the cosine similarity between the feature vector of the generated image and the average vector of the user’s original feature set.

**Diffusion Models.** For DreamBooth, we use Stable Diffusion version 2.1 (SD-v2.1). For Textual Inversion, we use Latent Diffusion models. We use LDMs to compute  $\mathcal{L}_{DM}$  in the first stage of TS-LFO.

**Implementation Details.** When optimizing latent features, we used the Adam optimizer with a learning rate set to  $5e-3$  and optimized for 3000 steps. For the CelebA-HQ dataset, we randomly selected 50 individuals, each of whom randomly selected 5 images. For the LSUN-cat and LSUN-sheep datasets, we randomly selected 50 individuals. For animal datasets lacking multiple images per individual, we augment each image through rotations at  $-10^\circ$ ,  $-5^\circ$ ,  $0^\circ$ ,  $5^\circ$ , and  $10^\circ$  to create 5 variants per identity. Next, we will use 5 images of the same individual to generate 50 images and compare the similarities and differences between the original clean images and the generated images, and then calculate their average. For all the methods mentioned above, we take their default parameters. For

**Table 2: (Textual Inversion) The performance of our method on SOTA defenses.**

Dataset	Metric	w/o def	AdvDM		SimAC		DisDiff	
			w/ def	TS-LFO	w/ def	TS-LFO	w/ def	TS-LFO
LSUN-cat	FID ↓	256.75	404.62	<b>284.33</b>	329.38	<b>269.47</b>	303.13	<b>267.34</b>
	CLIP <sub>img</sub> ↑	0.7902	0.6203	<b>0.7661</b>	0.7123	<b>0.7793</b>	0.7331	<b>0.7779</b>
	LPIPS ↓	0.6157	0.6701	<b>0.6275</b>	0.6483	<b>0.6282</b>	0.6330	<b>0.6327</b>
CelebA-HQ	FID ↓	187.86	256.91	<b>224.50</b>	286.98	<b>204.80</b>	205.94	<b>192.67</b>
	CLIP <sub>img</sub> ↑	0.7282	0.6212	<b>0.6603</b>	0.5983	<b>0.6807</b>	0.6769	<b>0.6973</b>
	LPIPS ↓	0.5175	0.6770	<b>0.6202</b>	0.6010	<b>0.5455</b>	0.5578	<b>0.5420</b>
LSUN-sheep	FID ↓	271.45	414.45	<b>294.34</b>	357.21	<b>290.08</b>	328.04	<b>291.39</b>
	CLIP <sub>img</sub> ↑	0.7494	0.5813	<b>0.7385</b>	0.6656	<b>0.7461</b>	0.6892	<b>0.7482</b>
	LPIPS ↓	0.6061	0.6651	<b>0.6233</b>	0.6556	<b>0.6296</b>	0.6441	<b>0.6266</b>

the DiffPure method, we set diffuse timestep as 100. For the adding Gaussian noise method, we set the mean to 0 and the standard deviation to 0.05. For all the defense methods mentioned above, we set the same noise budget of 16/255. All the experiments are conducted on NVIDIA GeForce RTX 3090 GPUs.

### 4.2 Main Experiments

This section validates the robustness of our proposed copyright attack against advanced defense mechanisms. We construct experiments on three datasets with distinct semantic differences: CelebA-HQ [17] (face dataset), LSUN-cat [39], and LSUN-sheep [39], to verify our generalization across different image distributions. As shown in Table 1 and Table 2, these defenses demonstrate significant effectiveness when not under attacks. Taking Textual Inversion as an example, we measure the average FID increase across three datasets (LSUN-cat, CelebA-HQ, LSUN-sheep) by subtracting the undefended baseline FID from the defended FID for each of the three SOTA defenses (AdvDM, SimAC, DisDiff). The resulting average increments are 119.97, 85.84, and 40.35, verifying the defenses’ ability to disrupt identifiable features, consistent with existing literature.

Notably, applying our TS-LFO causes substantial degradation of defense effectiveness. Taking Textual Inversion as an example, post-attack FID values recover to 267.72, 254.78, and 250.47 respectively, showing reductions of 90.94, 69.74, and 28.57 compared to defended FID averages of 358.66, 324.52, and 279.04. These consistent improvements across all defenses demonstrate that our method effectively mitigates the protection of existing defensive mechanisms, restoring the attack’s ability to generate identifiable images.

### 4.3 Attack Experiments on Face Dataset

To evaluate the efficacy of our TS-LFO method, we conducted experiments on the CelebA-HQ dataset, comparing against five copyright protection methods (i.e., PhotoGuard, Anti-DreamBooth, AdvDM, SimAC, and DisDiff) and four attack baselines (i.e., Gaussian Noise, IMPRESS, DiffPure, and GrIDPure). Results in Table 3 demonstrate that TS-LFO achieves superior balance between attack effectiveness and generation quality.

On the core metrics measuring generation utility, our method exhibits strong attack performance based on the FDFR metric. While TS-LFO’s FDFR values for defenses such as PhotoGuard, Anti-DreamBooth, and AdvDM are marginally higher than those of IMPRESS and Noise, they remain substantially lower than the

**Table 3: The performance of our method compared to the performance of SOTA copyright attacks on the CelebA-HQ dataset.**

Method	w/o def			PhotoGuard			Anti-DreamBooth			AdvDM			SimAC			DisDiff		
	FDFR	ISM	FID	FDFR	ISM	FID	FDFR	ISM	FID	FDFR	ISM	FID	FDFR	ISM	FID	FDFR	ISM	FID
w/o atk	0.1408	0.4650	172.4161	0.0360	0.3157	210.4718	0.1544	0.2563	364.3047	0.0836	0.2464	236.9997	0.2016	0.2843	306.7834	0.1636	0.4266	175.0311
Noise	-	-	-	<b>0.0812</b>	0.4365	178.0133	0.0828	0.4360	186.5673	0.0871	0.3435	206.6206	0.1076	0.4159	182.4842	0.1067	0.4566	176.6461
IMPRESS	-	-	-	0.0896	0.3272	189.2289	<b>0.0684</b>	0.3600	312.9439	<b>0.0400</b>	0.2831	235.0939	0.1276	0.3235	307.9065	0.1204	0.4406	184.1842
DiffPure	-	-	-	0.1024	0.4279	198.0258	0.1140	0.4281	202.8343	0.1580	0.3618	193.7353	0.1104	0.4202	205.4967	0.1528	0.4111	194.3153
GrIDDPure	-	-	-	0.1672	0.4101	183.0769	0.1036	0.4462	201.7735	0.1736	0.3395	184.0426	0.1340	0.4457	201.4953	0.1476	0.4405	193.5929
<b>TS-LFO</b>	<b>0.1029</b>	<b>0.4800</b>	<b>169.3565</b>	0.1012	<b>0.4487</b>	<b>171.6785</b>	0.0988	<b>0.4518</b>	<b>167.7494</b>	0.1084	<b>0.3686</b>	<b>181.3351</b>	<b>0.1060</b>	<b>0.4496</b>	<b>170.1528</b>	<b>0.1056</b>	<b>0.4668</b>	<b>165.8559</b>

**Table 4: Ablation Experiments on Timestep-Varying Weighting Coefficients.**

$\lambda_t$	0	$+\infty$	$1 \times 10^{-4}$	$3 \times 10^{-3}$	$1 \times 10^{-4} \sim 3 \times 10^{-3}$
FID ↓	241.73	260.59	237.20	231.55	<b>224.50</b>

original clean image baseline (0.1408). Moreover, under newer protections like SimAC and DisDiff, our approach significantly surpasses all baseline methods. Critically, even though TS-LFO was not optimized for autoencoder-based defenses (e.g., PhotoGuard), it achieves a notably lower FDFR (0.1012) than the unprotected clean image baseline, demonstrating that it not only removes perturbations but also actively enhances the latent representation to improve diffusion model compatibility.

On generation quality metrics, TS-LFO outperforms all baselines in both ISM and FID. For example, under PhotoGuard, TS-LFO attains an ISM of 0.4487 and FID of 171.6785, surpassing IMPRESS (ISM: 0.3272, FID: 189.2289). This highlights its ability to maintain high semantic fidelity while bypassing protections.

Furthermore, TS-LFO exhibits general image enhancement properties. When applied to clean images (w/o def), it improves all metrics: FDFR decreases to 0.1029, ISM increases to 0.4800, and FID reduces to 169.3565, confirming its role as an active representation optimizer rather than a mere perturbation filter.

Additionally, we observe that the Gaussian Noise method exhibits performance beyond expectations. Compared to other methods, Gaussian Noise not only shows certain advantages in the FDFR metric but also maintains decent performance in ISM and FID metrics. However, compared to our method, its FDFR does not show a significant advantage, and there remains a notable gap in ISM and FID metrics behind ours under the Anti-DreamBooth condition.

The attack results on more datasets are provided in Appendix B.1.

#### 4.4 Ablation Experiments

This section validates the necessity of each core component through ablation experiments conducted on the CelebA-HQ dataset with AdvDM as the defense baseline using Textual Inversion.

**Timestep-Varying Weighting Coefficients.** To verify the dynamic balancing mechanism between the Latent-Image Alignment Loss  $\mathcal{L}_{align}$  and the Latent Diffusion Loss  $\mathcal{L}_{DM}$ , we design five configurations. Through setting constant weight  $\lambda_t = 0$  to eliminate  $\mathcal{L}_{DM}$  and  $\lambda_t = +\infty$  to remove  $\mathcal{L}_{align}$ , we verify the necessity of both loss components. Additional experiments with static weights

**Table 5: Ablation Experiments on  $\epsilon_{rec}$  Parameter in Latent Reconstruction Stage.**

$\epsilon_{rec}$	4/255	<b>8/255</b>	12/255	255/255
FID ↓	248.39	<b>224.50</b>	227.77	230.16

**Table 6: Ablation Experiments on Metric Selection.**

Distance Metric	LPIPS	<b>MSE</b>	CLIP <sub>img</sub>	SSIM
FID ↓	235.94	<b>224.50</b>	243.21	248.13

$1 \times 10^{-4}$  and  $3 \times 10^{-3}$  demonstrate the need for dynamic adjustment. The proposed linear weight variation from  $1 \times 10^{-4}$  to  $3 \times 10^{-3}$  achieves the optimal FID score of 224.50 as shown in Table 4.

**$\epsilon_{rec}$  Parameter in Latent Reconstruction.** To validate the balancing effect of  $L_\infty$  constraint coefficient  $\epsilon_{rec}$  in Equation 8, we conduct experiments with four parameter settings. Disabling latent reconstruction by setting  $\epsilon_{rec} = 255/255$  confirms its necessity through a deteriorated FID value of 230.16. Comparative tests with  $\epsilon_{rec} = 4/255$  and  $12/255$  reveal the trade-off between feature quality and perturbation magnitude, while the proposed  $\epsilon_{rec} = 8/255$  configuration achieves optimal balance with an FID score of 224.50 as detailed in Table 5.

**Metric Selection Analysis.** In Table 6, our comparison of four similarity metrics for Latent-Image Alignment Loss  $\mathcal{L}_{align}$  reveals unexpected findings. While the perception-level metrics (i.e., SSIM, LPIPS) and the semantic-level CLIP<sub>img</sub> demonstrate better similarity, traditional pixel-wise MSE achieves superior performance with an FID score of 224.50. This counterintuitive result stems from advanced metrics misinterpreting adversarial perturbations as legitimate features during optimization.

**Table 7: Ablation Experiments on Optimization Steps.**

Optimization Steps	FDFR ↓	ISM ↑	FID ↓
1000	<b>0.0948</b>	0.4373	196.1289
2000	0.1500	0.4307	169.7964
<b>3000 (default)</b>	0.0988	<b>0.4518</b>	<b>167.7494</b>
4000	0.1296	0.4387	171.3990
5000	0.1104	0.4514	172.3843

**Optimization Steps Analysis.** We conduct an ablation study on optimization steps (1000~5000) to analyze its influence in Table 7. The experiments are conducted on the CelebA-HQ dataset using Dreambooth. With the steps rising from 1000 to 3000, FDFR first rises and then drops to the minimum (0.0988), ISM increases to the peak (0.4518), and FID decreases significantly to 167.7494, indicating better attack effectiveness, identity fidelity and generation quality. When the steps exceed 3000, FDFR rises, while ISM and FID fluctuate and degrade slightly, showing overfitting and unstable optimization. Overall, 3000 steps achieves the optimal trade-off between underfitting and overfitting, delivering the best comprehensive performance, which is set as the default configuration.

#### 4.5 Visualization Results and User Study

Due to the length constraint policy, the visualization and user study results are presented in Appendix B.2.

### 5 Conclusion

In this paper, we address the critical challenge of bypassing adversarial copyright defenses in diffusion-based customization by proposing the Two-Stage Latent Feature Optimization (TS-LFO) framework. Our investigation reveals that existing defense mechanisms rely on perturbing latent space representations to disrupt the alignment between input images and latent features to suppress personalized generation, leaving exploitable vulnerabilities.

The TS-LFO framework systematically recovers the compromised latent-image mapping through a two-stage approach: the latent denoising stage employs adaptive loss functions to eliminate high-frequency perturbations while preserving semantic consistency, and the latent reconstruction stage restores low-frequency structural details via pixel-level constraints. Extensive experiments validate that our method successfully bypasses state-of-the-art defenses across diverse settings, achieving high-fidelity content generation even when models are protected by adversarial perturbations.

This work marks an effective solution for circumventing copyright defenses in diffusion-based customization, challenging the robustness of current adversarial protection strategies. Our findings highlight the need for more sophisticated defense mechanisms that account for feature vulnerabilities in latent spaces.

**Limitations, Future Direction, and Social Impacts.** Although the TS-LFO method demonstrates stronger copyright attack capabilities, its requirement of 6 minutes to process a single  $512 \times 512$  image is indeed a drawback. However, compared to the DreamBooth training procedure (15 minutes) and the Textual Inversion training procedure (30 minutes), we argue that the time cost of the TS-LFO method is acceptable. Thus, TS-LFO remains a compelling choice for enhancing image generation quality. Moreover, TS-LFO bypasses protections including PhotoGuard, AdvDM, AntiDreamBooth, SimAC, and DisDiff, alerting the research community. We find that protection researchers often overlook robustness evaluation against advanced attacks, focusing instead on traditional ones. We hope our work serves as a benchmark for evaluating protection robustness and anticipate more robust defenses against TS-LFO in the future. Ultimately, this study underscores the importance of balancing copyright protection with open innovation in the era of

generative AI [24, 44], calling for collaborative efforts to establish ethical frameworks for responsible model customization.

### Acknowledgments

This work is supported in part by the National Natural Science Foundation of China under grant 62301189, 62576122, 62571298, Guangdong Basic and Applied Basic Research Foundation under grant 2026A1515011139.

### References

- [1] A. BLATTMANN, R. ROMBACH, H. LING, T. DOCKHORN, S. W. KIM, S. FIDLER, AND K. KREIS, *Align your latents: High-resolution video synthesis with latent diffusion models*, in Proceedings of the IEEE/CVF conference on computer vision and pattern recognition, 2023, pp. 22563–22575.
- [2] B. CAO, C. LI, T. WANG, J. JIA, B. LI, AND J. CHEN, *Impress: Evaluating the resilience of imperceptible perturbations against unauthorized data usage in diffusion-based generative ai*, Advances in Neural Information Processing Systems, 36 (2023), pp. 10657–10677.
- [3] H. CAO, C. TAN, Z. GAO, Y. XU, G. CHEN, P.-A. HENG, AND S. Z. LI, *A survey on generative diffusion models*, IEEE Transactions on Knowledge and Data Engineering, (2024).
- [4] B. CHEN, W. YU, Q. ZHANG, T. ZHUANG, H. WU, Y. JIANG, AND S.-T. XIA, *Editable-deeps: Reliable cross-modal semantic communications for facial editing*, arXiv preprint arXiv:2411.15702, (2024).
- [5] F.-A. CROITORU, V. HONDURU, R. T. IONESCU, AND M. SHAH, *Diffusion models in vision: A survey*, IEEE Transactions on Pattern Analysis and Machine Intelligence, 45 (2023), pp. 10850–10869.
- [6] J. DENG, J. GUO, E. VERVERAS, I. KOTSIA, AND S. ZAFEIRIOU, *Retinaface: Single-shot multi-level face localisation in the wild*, in Proceedings of the IEEE/CVF conference on computer vision and pattern recognition, 2020, pp. 5203–5212.
- [7] J. DENG, J. GUO, N. XUE, AND S. ZAFEIRIOU, *Arface: Additive angular margin loss for deep face recognition*, in Proceedings of the IEEE/CVF conference on computer vision and pattern recognition, 2019, pp. 4690–4699.
- [8] P. ESSER, J. CHIU, P. ATIGHEHCHIAN, J. GRANSKOG, AND A. GERMANIDIS, *Structure and content-guided video synthesis with diffusion models*, in Proceedings of the IEEE/CVF international conference on computer vision, 2023, pp. 7346–7356.
- [9] H. FANG, B. CHEN, X. WANG, Z. WANG, AND S.-T. XIA, *Gifd: A generative gradient inversion method with feature domain optimization*, in Proceedings of the IEEE/CVF International Conference on Computer Vision, 2023, pp. 4967–4976.
- [10] H. FANG, J. KONG, B. CHEN, T. DAI, H. WU, AND S.-T. XIA, *Clip-guided generative networks for transferable targeted adversarial attacks*, in European Conference on Computer Vision, Springer, 2024, pp. 1–19.
- [11] H. FANG, J. KONG, W. YU, B. CHEN, J. LI, H. WU, S.-T. XIA, AND K. XU, *One perturbation is enough: On generating universal adversarial perturbations against vision-language pre-training models*, in Proceedings of the IEEE/CVF International Conference on Computer Vision, 2025, pp. 4090–4100.
- [12] H. FANG, Y. QIU, H. YU, W. YU, J. KONG, B. CHONG, B. CHEN, X. WANG, S.-T. XIA, AND K. XU, *Privacy leakage on dnns: A survey of model inversion attacks and defenses*, arXiv preprint arXiv:2402.04013, (2024).
- [13] H. FANG, W. YU, B. CHEN, X. WANG, S.-T. XIA, Q. LIAO, AND K. XU, *Enhancing gradient inversion attacks in federated learning via hierarchical feature optimization*, arXiv preprint arXiv:2604.00955, (2026).
- [14] R. GAL, Y. ALALUF, Y. ATZMON, O. PATASHNIK, A. H. BERMANO, G. CHECHIK, AND D. COHEN-OR, *An image is worth one word: Personalizing text-to-image generation using textual inversion*, in The Eleventh International Conference on Learning Representations.
- [15] R. GAL, Y. ALALUF, Y. ATZMON, O. PATASHNIK, A. H. BERMANO, G. CHECHIK, AND D. COHEN-OR, *An image is worth one word: Personalizing text-to-image generation using textual inversion*, arXiv preprint arXiv:2208.01618, (2022).
- [16] M. HEUSEL, H. RAMSAUER, T. UNTERTHINER, B. NESSLER, AND S. HOCHREITER, *Gans trained by a two time-scale update rule converge to a local nash equilibrium*, Advances in neural information processing systems, 30 (2017).
- [17] T. KARRAS, T. AILA, S. LAINE, AND J. LEHTINEN, *Progressive growing of gans for improved quality, stability, and variation*, arXiv preprint arXiv:1710.10196, (2017).
- [18] B. KAWAR, S. ZADA, O. LANG, O. TOV, H. CHANG, T. DEKEL, I. MOSSERI, AND M. IRANI, *Imagic: Text-based real image editing with diffusion models*, in Proceedings of the IEEE/CVF conference on computer vision and pattern recognition, 2023, pp. 6007–6017.
- [19] C. LIANG, X. WU, Y. HUA, J. ZHANG, Y. XUE, T. SONG, Z. XUE, R. MA, AND H. GUAN, *Adversarial example does good: Preventing painting imitation from diffusion models via adversarial examples*, arXiv preprint arXiv:2302.04578, (2023).
- [20] X. LIU, D. H. PARK, S. AZADI, G. ZHANG, A. CHOPIKYAN, Y. HU, H. SHI, A. ROHRBACH, AND T. DARRELL, *More control for free! image synthesis with semantic diffusion guidance*, in Proceedings of the IEEE/CVF winter conference on

- applications of computer vision, 2023, pp. 289–299.
- [21] Y. LIU, J. AN, W. ZHANG, D. WU, J. GU, Z. LIN, AND W. WANG, *Disrupting diffusion: Token-level attention erasure attack against diffusion-based customization*, in Proceedings of the 32nd ACM International Conference on Multimedia, 2024, pp. 3587–3596.
- [22] W. NIE, B. GUO, Y. HUANG, C. XIAO, A. VAHDAT, AND A. ANANDKUMAR, *Diffusion models for adversarial purification*, in International Conference on Machine Learning, PMLR, 2022, pp. 16805–16827.
- [23] B. POOLE, A. JAIN, J. T. BARRON, AND B. MILDENHALL, *Dreamfusion: Text-to-3d using 2d diffusion*, arXiv preprint arXiv:2209.14988, (2022).
- [24] R. QIAO, Q. TAN, P. YANG, Y. WANG, X. WANG, E. WAN, G. DONG, S. LANG, S. ZHOU, Y. XU, Y. ZENG, J. WANG, C. SUN, C. LI, AND H. ZHANG, *We-math 2.0: A versatile mathbook system for incentivizing visual mathematical reasoning*, in The Fourteenth International Conference on Learning Representations, 2026.
- [25] Y. QIU, H. FANG, H. YU, B. CHEN, M. QIU, AND S.-T. XIA, *A closer look at gan priors: Exploiting intermediate features for enhanced model inversion attacks*, in European Conference on Computer Vision, Springer, 2024, pp. 109–126.
- [26] Y. QIU, H. YU, H. FANG, W. YU, B. CHEN, X. WANG, S.-T. XIA, AND K. XU, *Mibench: A comprehensive benchmark for model inversion attack and defense*, (2024).
- [27] A. RADFORD, J. W. KIM, C. HALLACY, A. RAMESH, G. GOH, S. AGARWAL, G. SASTRY, A. ASKELL, P. MISHKIN, J. CLARK, ET AL., *Learning transferable visual models from natural language supervision*, in International conference on machine learning, PmlR, 2021, pp. 8748–8763.
- [28] R. ROMBACH, A. BLATTMANN, D. LORENZ, P. ESSER, AND B. OMMER, *High-resolution image synthesis with latent diffusion models*, in Proceedings of the IEEE/CVF conference on computer vision and pattern recognition, 2022, pp. 10684–10695.
- [29] O. RONNEBERGER, P. FISCHER, AND T. BROX, *U-net: Convolutional networks for biomedical image segmentation*, in Medical image computing and computer-assisted intervention–MICCAI 2015: 18th international conference, Munich, Germany, October 5–9, 2015, proceedings, part III 18, Springer, 2015, pp. 234–241.
- [30] N. RUIZ, Y. LI, V. JAMPANI, Y. PRITCH, M. RUBINSTEIN, AND K. ABERMAN, *Dreambooth: Fine tuning text-to-image diffusion models for subject-driven generation*, in Proceedings of the IEEE/CVF conference on computer vision and pattern recognition, 2023, pp. 22500–22510.
- [31] H. SALMAN, A. KHADDAJ, G. LECLERC, A. ILYAS, AND A. MADRY, *Raising the cost of malicious ai-powered image editing*, arXiv preprint arXiv:2302.06588, (2023).
- [32] Y. TAKAGI AND S. NISHIMOTO, *High-resolution image reconstruction with latent diffusion models from human brain activity*, in Proceedings of the IEEE/CVF Conference on Computer Vision and Pattern Recognition, 2023, pp. 14453–14463.
- [33] Y. TAN, Y. PENG, H. FANG, B. CHEN, AND S.-T. XIA, *Waterdiff: Perceptual image watermarks via diffusion model*, in ICASSP 2024–2024 IEEE International Conference on Acoustics, Speech and Signal Processing (ICASSP), IEEE, 2024, pp. 3250–3254.
- [34] T. VAN LE, H. PHUNG, T. H. NGUYEN, Q. DAO, N. N. TRAN, AND A. TRAN, *Anti-dreambooth: Protecting users from personalized text-to-image synthesis*, in Proceedings of the IEEE/CVF International Conference on Computer Vision, 2023, pp. 2116–2127.
- [35] F. WANG, Z. TAN, T. WEI, Y. WU, AND Q. HUANG, *Simac: A simple anti-customization method for protecting face privacy against text-to-image synthesis of diffusion models*, in Proceedings of the IEEE/CVF Conference on Computer Vision and Pattern Recognition, 2024, pp. 12047–12056.
- [36] Z. WANG, C. CHEN, L. LYU, D. N. METAXAS, AND S. MA, *Diagnosis: Detecting unauthorized data usages in text-to-image diffusion models*, in The Twelfth International Conference on Learning Representations.
- [37] H. XIAO, W. YU, H. FANG, S. SUN, B. CHEN, X. WANG, AND S.-T. XIA, *Diffusion-based natural adversarial perturbations towards segment anything model*, in ICASSP 2026–2026 IEEE International Conference on Acoustics, Speech and Signal Processing (ICASSP), IEEE, 2026, pp. 13637–13641.
- [38] L. YANG, Z. ZHANG, Y. SONG, S. HONG, R. XU, Y. ZHAO, W. ZHANG, B. CUI, AND M.-H. YANG, *Diffusion models: A comprehensive survey of methods and applications*, ACM Computing Surveys, 56 (2023), pp. 1–39.
- [39] F. YU, A. SEFF, Y. ZHANG, S. SONG, T. FUNKHOUSER, AND J. XIAO, *Lsun: Construction of a large-scale image dataset using deep learning with humans in the loop*, arXiv preprint arXiv:1506.03365, (2015).
- [40] W. YU, B. CHEN, Q. ZHANG, AND S.-T. XIA, *Editable-deeps: cross-modal editable semantic communication systems*, in 2024 IEEE 99th Vehicular Technology Conference (VTC2024-Spring), IEEE, 2024, pp. 1–5.
- [41] W. YU, H. FANG, B. CHEN, X. SUI, C. CHEN, H. WU, S.-T. XIA, AND K. XU, *Gi-nas: Boosting gradient inversion attacks through adaptive neural architecture search*, IEEE Transactions on Information Forensics and Security, (2025).
- [42] R. ZHANG, P. ISOLA, A. A. EFROS, E. SHECHTMAN, AND O. WANG, *The unreasonable effectiveness of deep features as a perceptual metric*, in Proceedings of the IEEE conference on computer vision and pattern recognition, 2018, pp. 586–595.
- [43] Y. ZHANG, *A better autoencoder for image: Convolutional autoencoder*, in ICONEP17-DCEC. Available online: [http://users.cecis.anu.edu.au/Tom.Gedeon/conf/ABCs2018/paper/ABCs2018\\_paper\\_58.pdf](http://users.cecis.anu.edu.au/Tom.Gedeon/conf/ABCs2018/paper/ABCs2018_paper_58.pdf) (accessed on 23 March 2017), 2018.
- [44] Y. ZHANG, Y. HUANG, Y. SUN, C. LIU, Z. ZHAO, Z. FANG, Y. WANG, H. CHEN, X. YANG,

X. WEI, ET AL., *Multitrust: A comprehensive benchmark towards trustworthy multimodal large language models*, Advances in Neural Information Processing Systems, 37 (2024), pp. 49279–49383.

- [45] Z. ZHAO, J. DUAN, K. XU, C. WANG, R. ZHANG, Z. DU, Q. GUO, AND X. HU, *Can protective perturbation safeguard personal data from being exploited by stable diffusion?*, in Proceedings of the IEEE/CVF Conference on Computer Vision and Pattern Recognition, 2024, pp. 24398–24407.

## A Algorithm of our method

Our TS-LFO framework is outlined in Fig. 4. While the main manuscript assumes deterministic latent feature  $z$  from autoencoder, practical implementations may involve probabilistic encoders like variational autoencoders (VAEs) that output Gaussian distribution parameters  $(\mu, \sigma)$ . To ensure compatibility, we further develop Alg. 1, extending the optimization from deterministic  $z$  to latent distribution parameters. This enhanced version maintains TS-LFO’s core objective: *reconstructing the mapping between input images and latent space while supporting diverse autoencoder architectures*.

## B More Experimental Results

### B.1 Attack Experiments on More Datasets

To comprehensively evaluate the attack effectiveness of our method, we design a cross-defense and cross-domain experimental framework. This experimental setup contains two comparative dimensions. In the defense strategy dimension, we select four SOTA defense paradigms: Anti-DreamBooth, AdvDM, SimAC, and DisDiff. In the attack method dimension, we compare our approach against four baseline categories: SOTA adversarial purification DiffPure, SOTA copyright attack methods including IMPRESS and GrIDPure, and traditional defense Gaussian noise.

Experimental results in Table 8 reveal two critical findings. First, our method demonstrates superior attack performance. On CelebA-HQ against SimAC defense, our method achieves an FID score of 170.15, outperforming DiffPure and GrIDPure by margins of 35.35 and 31.35, respectively. On LSUN-cat, our FID value of 247.57 significantly surpasses the suboptimal DiffPure with a 3.8 improvement.

Furthermore, the traditional Gaussian noise method shows unexpected performance. On the CelebA-HQ dataset, this method can even surpass the SOTA copyright attack methods to become the second-best method behind our TS-LFO. This indicates that there is still great potential for improvement in the performance of current copyright attack and protection methods.

**Table 8: (DreamBooth) The FID performance of our method compared to the performance of SOTA copyright attacks on more datasets.**

Defense	Dataset	w/o def	w/ def	Attack				
				Noise	IMPRESS	DiffPure	GrIDPure	TS-LFO
Anti-DreamBooth	LSUN-cat	234.52	339.78	267.39	333.06	249.28	274.79	<b>243.62</b>
	CelebA-HQ	172.42	364.30	186.57	312.94	202.83	201.77	<b>167.75</b>
	LSUN-sheep	297.63	369.24	322.08	366.46	307.01	335.40	<b>303.08</b>
AdvDM	LSUN-cat	234.52	401.08	334.16	398.40	255.95	319.12	<b>249.94</b>
	CelebA-HQ	172.42	237.00	206.62	235.09	193.74	184.04	<b>181.34</b>
	LSUN-sheep	297.63	417.33	385.16	417.01	311.20	355.94	<b>306.16</b>
SimAC	LSUN-cat	234.52	362.01	274.19	364.37	251.37	280.06	<b>247.57</b>
	CelebA-HQ	172.42	306.78	182.48	307.91	205.50	201.50	<b>170.15</b>
	LSUN-sheep	297.63	414.84	331.21	419.27	305.03	328.96	<b>301.74</b>
DisDiff	LSUN-cat	234.52	327.16	261.42	330.64	248.47	287.11	<b>244.12</b>
	CelebA-HQ	172.42	175.03	176.65	184.18	194.32	193.59	<b>165.86</b>
	LSUN-sheep	297.63	395.20	325.26	387.59	308.40	337.86	<b>304.83</b>

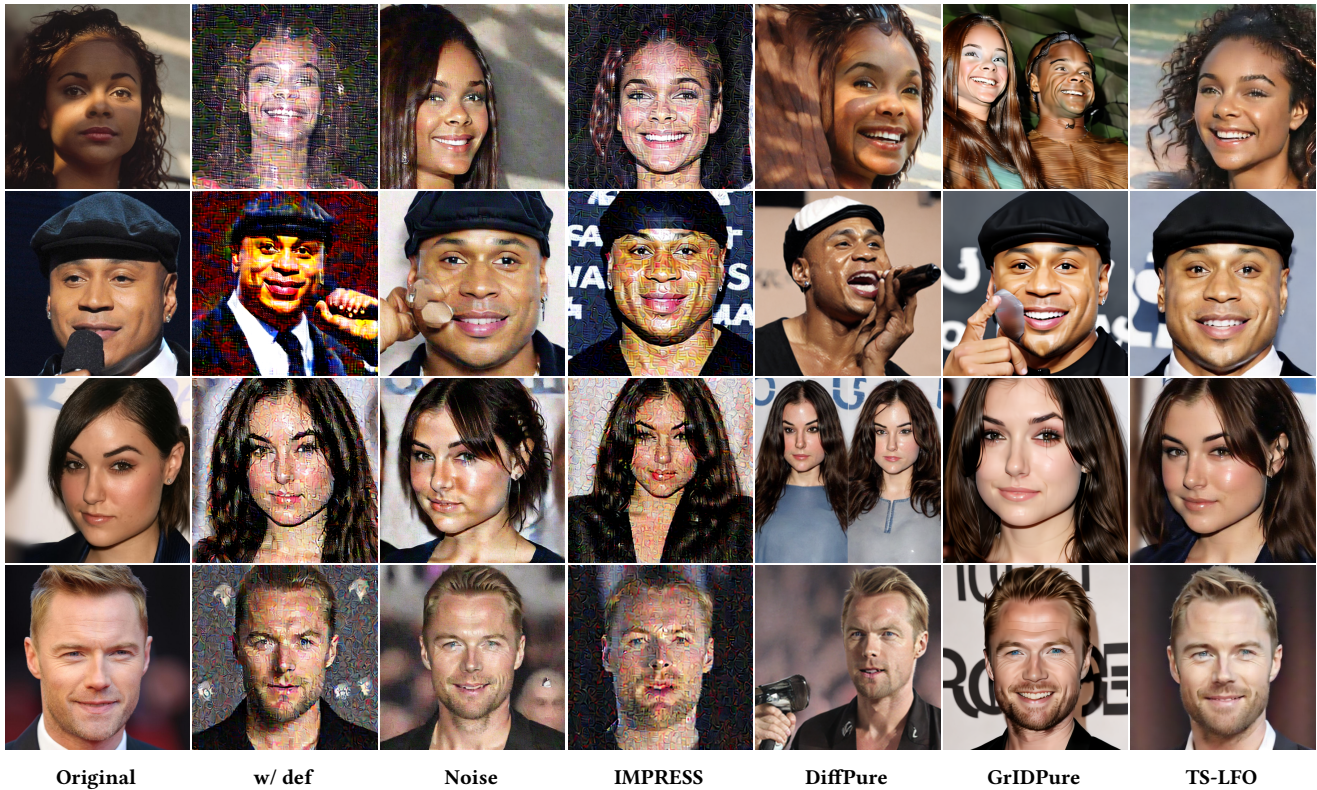


Figure 6: Visualized comparison of images generated by different copyright attacks with the original images under the copyright protection of Anti-Dreambooth and SimAC.

Table 9: The proportion of selected samples by users on Dreambooth.

Defense	w/def	Noise	IMPRESS	DiffPure	GrIDPure	TS-LFO
Anti-Dreambooth	8.8%	49.4%	18.1%	43.8%	40.6%	71.9%
SimAC	15.0%	36.9%	16.3%	28.8%	63.8%	78.1%

### B.2 Visualization Results and User Study

**Visualization Results.** We provide the visualized comparison of different methods in Fig. 6. From Fig. 6, we observe that our method has successfully learned original image features under all the protection schemes. Compared with the other copyright attack methods, TS-LFO can generate images with significantly higher similarity to the original ones.

**User Study.** We also conduct the user study to further evaluate the image quality. Specifically, we recruited 100 users and invited them to rate the generated images of different methods. Each user was provided with the following textual instruction: “Which images are of the best quality and most similar to the reference (clean) image? Please select 2 to 4 images.” Then, we analyzed the proportion of samples selected for each method in Table 9. We notice that our TS-LFO has again surpassed all the other methods in the user study.

### B.3 Experiments about Semantic-Level Copyright Protection

In previous experiments, we only evaluated the performance of TS-LFO in pixel-level adversarial noise-based copyright protections. Some methods such as DIAGNOSIS [36] embed robust watermark signals, generally through semantic-level changes, which may not be attacked. To test the effectiveness of our method against the DIAGNOSIS protection, we conducted the following experiments:

- First, we randomly selected 50 groups of individuals from the CelebA-HQ dataset, with 5 images per group, totally 250 images. These 250 images were protected using the DIAGNOSIS method, resulting in 250 protected images. Using the 250 original images and 250 protected images, we trained a binary classifier for 200 epochs (400 images for the training dataset and 100 images for the validation dataset).
- We then tested the performance of this classifier, and the results are shown in Table 10. On the 500 images originally used

**Table 10: The accuracy of the trained classifier in determining whether an image contains a DIAGNOSIS watermark.**

Metric	train+val	test
prec $\uparrow$	97.20%	92.40%

**Table 11: The percentage of images flagged with the DIAGNOSIS watermark by the classifier in Table 10.**

Metric	original	protected	attacked
percentage $\uparrow$	2.32%	17.24%	0.92%

for training (training and validation datasets), the accuracy reached 97.20%. To further test the classifier’s performance, we randomly selected another 50 groups of individuals from CelebA-HQ, obtaining 500 test images in a similar way (test set), and the classifier achieved an accuracy of 92.40% on these images. This sufficiently demonstrates the superior performance of the trained classifier on the DIAGNOSIS.

- Next, we used the TS-LFO method to perform a copyright attack on the 250 protected images, obtaining 250 attacked images. The 250 original images were divided into 50 groups (5 images per group), and we used DreamBooth to fine-tune a diffusion model, generating 50 images per group, totally 2,500 generated images. These generated images were fed into the classifier to test what percentage of them were classified as containing the DIAGNOSIS semantic watermark. We performed a similar process for the 250 protected images and the 250 attacked images. The experimental results are shown in Table 11.
- For the images generated from the original images, only 2.32% were classified by the classifier as containing the DIAGNOSIS semantic watermark. In contrast, for the images generated from the protected images, 17.24% were classified as containing the DIAGNOSIS watermark. This indicates that the DIAGNOSIS defense significantly increases the probability of the generator producing images with the semantic watermark embedded. (Note: In the DIAGNOSIS paper, this ratio was 100% rather than 17.24%. This discrepancy arises because the DIAGNOSIS authors only experimented with LoRA and LoRA+DreamBooth generative models, not the standalone DreamBooth model we used here. Additionally, DIAGNOSIS typically fine-tunes diffusion models using hundreds to tens of thousands of images, whereas we used only 5 images per group to fine-tune the model. Fine-tuning with just 5 images was insufficient for the diffusion model to fully learn the characteristics of the semantic watermark.)
- After applying TS-LFO, this proportion decreased to 0.92%, even lower than the baseline from the original images. This demonstrates that TS-LFO can effectively attack the DIAGNOSIS copyright defense method.

**Algorithm 1** TS-LFO Variant with Gaussian Latent Distribution**Require:**

- 1:  $N$ : Number of training steps
- 2:  $x_{adv}$ : Adversarially perturbed input image
- 3:  $E(\cdot)$ : Encoder outputting Gaussian parameters  $(\mu, \sigma)$
- 4:  $D(\cdot)$ : Pre-trained LDM decoder
- 5:  $\epsilon_{\theta}(\cdot)$ : Pre-trained Unet denoiser
- 6:  $M(\cdot, \cdot)$ : An image similarity metric
- 7:  $T$ : Total diffusion timesteps
- 8:  $\eta$ : Learning rate
- 9:  $\lambda_l, \lambda_r$ : Initial/Final weight factors
- 10:  $\epsilon_{rec}$ : Reconstruction threshold

**Ensure:**

- 11:  $z_{new}$ : Optimized latent feature
- 12: **procedure** TS-LFO-GAUSSIAN( $N, x_{adv}, E, D, \epsilon_{\theta}, M, T, \eta, \lambda_l, \lambda_r, \epsilon_{rec}$ )
- 13:    // Stage 1: Latent Denoising
- 14:    // Initial distribution parameters
- 15:     $(\mu, \sigma) \leftarrow E(x_{adv})$
- 16:    **for**  $i = 1$  **to**  $N$  **do**
- 17:       Sample  $t$  from  $[1, T]$  randomly
- 18:       // Reparameterization
- 19:       Sample  $z \sim \mathcal{N}(\mu, \sigma^2)$
- 20:       // Compute  $\alpha_t$  via noise schedule
- 21:        $z_t \leftarrow \sqrt{\alpha_t}z + \sqrt{1 - \alpha_t}\epsilon$
- 22:       // Loss Computation
- 23:        $\mathcal{L}_{align} \leftarrow M(D(z), x_{adv})$
- 24:        $\mathcal{L}_{DM} \leftarrow \|\epsilon - \epsilon_{\theta}(z_t, t, c)\|_2^2$
- 25:        $\lambda_t \leftarrow \lambda_l + \frac{(\lambda_r - \lambda_l)}{T} \cdot t$
- 26:        $\mathcal{L}_{total} \leftarrow \mathcal{L}_{align} + \lambda_t \mathcal{L}_{DM}$
- 27:       // Distribution Update
- 28:        $\nabla_{\mu} \leftarrow \frac{\partial \mathcal{L}_{total}}{\partial \mu}$
- 29:        $\nabla_{\sigma} \leftarrow \frac{\partial \mathcal{L}_{total}}{\partial \sigma}$
- 30:       // Update mean
- 31:        $\mu \leftarrow \mu - \eta \nabla_{\mu}$
- 32:       // Update std dev
- 33:        $\sigma \leftarrow \sigma - \eta \nabla_{\sigma}$
- 34:     **end for**
- 35:    // Stage 2: Latent Reconstruction
- 36:    // Final sampling
- 37:    Sample  $z \sim \mathcal{N}(\mu, \sigma^2)$
- 38:     $x_{rec} \leftarrow \text{clamp}(D(z), x_{adv} - \epsilon_{rec}, x_{adv} + \epsilon_{rec})$
- 39:    // Re-encode with new distribution
- 40:     $z_{new} \leftarrow E(x_{rec}).\text{sample}()$
- 41:    **return**  $z_{new}$
- 42: **end procedure**